RESEARCH ON THE DYNAMICS OF A HEAVY MECHANIZED BRIDGE IN THE DEPLOYMENT PHASE OF THE LIFTING FRAME

Tran Duc Thang✉
Institute of Vehicle and Energy Engineering[1]
thangdt135@mta.edu.vn

Duong Van Le
Institute of Vehicle and Energy Engineering[1]

Dat Van Chu
Institute of Vehicle and Energy Engineering[1]

[1]Le Quy Don Technical University
236 Hoang Quoc Viet, Hanoi, Vietnam, 100000

✉Corresponding author

Abstract

This article presents a dynamic model of the TMM-3M heavy mechanized bridge during the frame lifting stage, which is driven by a hydraulic system, constituting the initial phase of the bridge erection process. The model is constructed as a multi-body dynamic system, taking into account the elastic deformation of the rear outriggers, front tires, and front suspension system. The research model integrates a mechanical system controlled by hydraulic cylinders, with pressure being considered as a variable reacting to external loads during the system's operation. Lagrangian equations of the second kind are utilized to establish a system of differential equations describing the oscillations of the system and form the basis for investigating the dynamics of the frame lifting process. The system of differential equations is solved numerically using MATLAB simulation software based on the Runge-Kutta algorithm. The study has revealed laws regarding the displacement and velocity of components within the system, evaluating the stability of the TMM-3M heavy mechanized bridge during operation. This research paves the way for a comprehensive understanding of the working process of the TMM-3M heavy mechanized bridge, aiming for practical improvements to minimize deployment or retrieval time, reduce the number of deployment team members, enhance the automation of the operation process to reduce the workload for operators.

Keywords: military bridge, dynamic, heavy mechanized bridge, hydraulic cylinder, mechanical-hydraulic.

1. Introduction

Heavy mechanized bridges are specialized equipment designed for both military and civilian applications to facilitate the rapid deployment of temporary bridges. These bridges are used to establish mobile routes for vehicles and people, enabling them to overcome obstacles such as shallow gaps, rivers, or other barriers. The heavy mechanized bridges are typically deployed by engineering units within the armed forces of various nations. In civilian settings, they are often part of search and rescue units. The production and utilization of heavy mechanized bridges, especially since the 1960s, have been notable in countries such as the United States, India, Germany, Russia, the Czech Republic, China, Finland, Poland, and others [1–8]. The base vehicles for these devices can be wheeled or tracked. Scientific publications on heavy mechanized bridges remain limited up to the present time. This limitation is partly attributed to the classified nature of military operations in different nations and the infrequent civilian use of such equipment.

The heavy mechanized bridge TMM-3M in **Fig. 1** is a representative example of heavy mechanized bridges with a wheeled chassis. Manufactured by the former Soviet Union since the 1970s, it continues to be effectively utilized by several countries. Numerous improvements have been implemented to enhance the technical capabilities and operational efficiency of this equipment. The deployment process of the TMM-3M heavy mechanized bridge consists of four main stages in the following order:

the frame lifting stage, the bridge span opening stage, the bridge span lowering stage, and the intermediate support leg lowering stage. During the frame lifting stage, the lifting cylinders operate to transition the entire bridge span from a horizontal position on the chassis to an upright standing position. Simultaneously, in this stage, the main cable system on the equipment remains inactive.

Fig. 1. The heavy mechanized bridge TMM-3M [9]

When researching the deployment process of the heavy mechanized bridge TMM-3M during the frame lifting stage, similarities can be observed with the operations of other machinery such as self-dumping trucks, wheeled cranes, and wheeled excavators. Dynamics studies closely related to the frame lifting stage in deploying bridge equipment, including the dynamics of self-dumping trucks during unloading, the dynamics of equipment on hydraulic excavators, have attracted attention from scientists and resulted in numerous publications. Research on the unloading process of dump trucks, where the lifting of the body is considered as a static process to determine the maximum tipping angle, was conducted in the study [10]. A similar study was conducted in [11], where the authors investigated the structure of the body lifting mechanism to optimize its design. In [12], the authors discussed the calculation of the lifting mechanism on dump trucks, with a focus on hydraulic cylinder calculations for lifting and lowering the body. In the study [13], the authors established a multi-body dynamics model of a dump truck using SIMPACK software, providing displacement, velocity, and acceleration results for various stages, although without theoretical calculations. In [14], a nonlinear model of the lifting and rolling process of dump trucks was established by considering the influence of elastic deformation of tires, suspension systems, and torsional deformation of cargo boxes on the rolling movement of the vehicle. In [15], the authors presented the oscillation of a hydraulic boom suspended freely during rotation, highlighting the significant influence of hydraulic valve control on the operational process. Research on anti-swing control for hydraulic boom cranes was addressed in [16], which also discussed the impact of cylinder pressure. In a specific study [17], the author developed a hydraulic-driven mechanical system model for a wheel loader, where the pushing force of the hydraulic cylinder varied based on external loads. However, this model does not include a front suspension system, unlike the Kraz255B chassis on the heavy mechanized bridge TMM-3M. Some research models treat the hydraulic cylinder as a resilient shock-absorbing spring, while others consider the pushing force of the cylinder as constant [18–20].

A comprehensive study of the working process of the heavy mechanized bridge TMM-3M in the stage of lifting the specialized working equipment assembly, comprising the lifting frame,

bridge span, and intermediate support leg, has not been published. In this paper, the author conducts a dynamic analysis of the heavy mechanized bridge TMM-3M during the deployment stage, specifically focusing on the frame lifting process. The results of this study serve as a basis for designing and improving the hydraulic lifting system for bridge spans, replacing the original mechanical rear outriggers with hydraulic ones to find a solution for reducing deployment time, enhancing the automation capability of the working process, and reducing the number of operating members.

2. Materials and methods
2. 1. System description

The process of lifting the frame during the deployment of the heavy mechanized bridge TMM-3M is carried out with the based vehicle in a stationary condition. During the frame lifting, the based vehicle stands on an absolutely rigid surface, and the two rear outriggers legs are lowered to the ground to address the lateral and longitudinal slopes of the terrain. At this point, the rear axle of the vehicle chassis does not influence the oscillation of the equipment.

During this process, the bridge span, lifting frame, and intermediate support leg are rigidly connected to form a unified block using clamps and connecting pins, collectively referred to as the bridge span block. The lifting cylinder activates the lifting frame to generate a pushing force, lifting the entire bridge span block from a horizontally positioned state on the vehicle chassis to an upright standing position, gradually straightening the two linkages. The masses are considered absolutely rigid and placed at the center of gravity of each section, including the non-suspended front axle mass m_1, the suspended mass on the vehicle chassis m_2, and the mass of the bridge span block m_s.

The dynamic analysis model of the heavy mechanized bridge during the frame lifting stage is a flat model, as illustrated in **Fig. 2**.
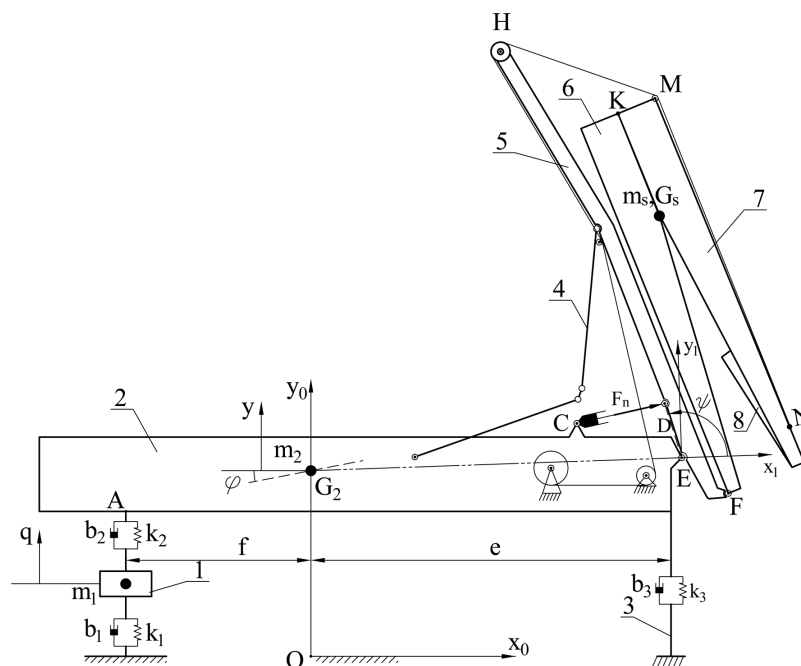

Fig. 2. Dynamic model of the heavy mechanized bridge during the frame lifting stage:
1 – front axle; 2 – chassis; 3 – rear outriggers; 4 – linkages; 5 – lifting frame; 6 – front half-span of the bridge; 7 – rear half-span of the bridge; 8 – intermediate bridge support

Wind load effects on the frame lifting process are disregarded in this model. In this model, the only external force is the pushing force of the hydraulic cylinder, which induces a moment causing the bridge span block to rotate. The entire mechanical system is placed within the fixed coordinate system Ox_0y_0. The vehicle body performs simultaneous translational motion along the vertical axis and tilts about an axis passing through the center of mass, perpendicular to the symmetric vertical

plane of the chassis. The bridge span block undergoes rotational motion around the hinge joint E, connecting the bridge span block and chassis.

Besides the remaining geometric dimensions described in **Fig. 2**, several other symbols are conventionally defined as follows: b_1, k_1 respectively represent the damping coefficient and stiffness coefficient of the front tires; b_2, k_2 respectively represent the damping coefficient and stiffness coefficient of the front suspension system; b_3, k_3 respectively represent the damping coefficient and stiffness coefficient of the rear outriggers; G_1, G_2, G_s correspondingly represent the center of mass positions of masses m_1, m_2, m_s in a system; J_2, J_s respectively represent the moments of inertia of the body vehicle and the bridge span block; H_1, H_2 respectively represent the initial heights of the center of mass of masses m_1 and m_2.

The distances are denoted as follows:

$$n_1 = EG_2; n_2 = CG_2; n_3 = ED; n_4 = EG_s; n_5 = EC;$$

$$\alpha_1 = \angle EG_2L; \alpha_2 = \angle CG_2L; \alpha_3 = \angle DEG_s; \alpha_4 = \angle CEG_2.$$

In which G_2L always has a vertical direction along the chassis.

2. 2. Motion equations
2. 2. 1. Generalized coordinates
Generalized coordinates have been assumed whose vector (**Fig. 2**) has the form:

$$\begin{bmatrix} q & y & \varphi & \psi \end{bmatrix}^T, \tag{1}$$

where $q(m)$ – vertical displacement of the unsprung mass of the front axle; $y(m)$ – vertical displacement of the center of mass of the chassis; $\varphi(rad)$ – pitch angle of the chassis; $\psi(rad)$ – angular displacement of the bridge span block.

2. 2. 2. The kinetic energy of the system
The kinetic energy of the system includes the kinetic energy of the unsprung mass of the front axle, the kinetic energy of the suspended mass on the chassis, the kinetic energy of the bridge span block, and is determined by the expression:

$$T = \frac{1}{2}m_1\dot{q}^2 + \frac{1}{2}m_2\dot{y}^2 + \frac{1}{2}J_2\dot{\varphi}^2 + \frac{1}{2}J_s\dot{\psi}^2 +$$
$$+\frac{1}{2}m_s\left\{\begin{matrix} n_1^2\dot{\varphi}^2 + \dot{y}^2 + n_4^2(\dot{\varphi}+\dot{\psi})^2 + 2n_1n_4\cos(\psi+\alpha_3-\alpha_1)(\dot{\varphi}+\dot{\psi})\dot{\varphi} + \\ +2n_1\cos(\varphi+\alpha_1)\dot{\varphi}\dot{y} + 2n_4\cos(\varphi+\psi+\alpha_3)(\dot{\varphi}+\dot{\psi})\dot{y} \end{matrix}\right\}. \tag{2}$$

2. 2. 3. The potential energy of the system
The potential energy of the system includes gravitational potential energy and elastic potential energy.

There is the expression defining the total potential energy of the system as:

$$\Pi = \left\{\begin{matrix} m_1g(q+H_1) + m_2g(y+H_2) + m_sg\begin{pmatrix} y+H_2+n_1\sin(\varphi+\alpha_1)+ \\ +n_4\sin(\varphi+\psi+\alpha_3) \end{pmatrix} + \\ +\frac{1}{2}k_2(y-q-f\varphi)^2 + \frac{1}{2}k_1q^2 + \frac{1}{2}k_3(y+e\varphi)^2 \end{matrix}\right\}. \tag{3}$$

2. 2. 4. The total dissipative energy of the system
The total dissipative energy of the system is determined by the following expression:

$$\Phi = \frac{1}{2}b_2(\dot{y}-\dot{q}-f\dot{\varphi})^2 + \frac{1}{2}b_1\dot{q}^2 + \frac{1}{2}b_3(\dot{y}+e\dot{\varphi})^2. \tag{4}$$

2. 2. 5. Generalized forces

The visual work done by external forces acting on the system is: the pushing force (F_n) of the hydraulic cylinder at any given moment causing the rotation of the bridge span block by an angle ψ. The potential displacement work at that moment can be expressed as:

$$\delta A = F_n r \delta \psi. \tag{5}$$

In which r is the distance from E to the line of action of the force vector $\vec{F}_n$, and is determined by the expression:

$$r = \frac{n_3 n_5 \sin\left(\psi + \alpha_4\right)}{\sqrt{n_1^2 + n_2^2 + n_3^2 - 2n_1 n_2 \cos\left(\alpha_2 - \alpha_1\right) + 2n_1 n_3 \cos\left(\psi - \alpha_1\right) - 2n_2 n_3 \cos\left(\psi - \alpha_2\right)}}. \tag{6}$$

The pushing force of the hydraulic cylinder is caused by the pressure in the cylinder chamber. This pressure varies according to the external load acting on the piston rod and the displacement speed of the piston. To determine the pressure and pushing force of the hydraulic cylinder, let's consider the following simple hydraulic cylinder model (**Fig. 3**).
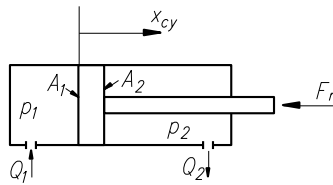

Fig. 3. Sketch model of Hydraulic cylinder

The equation for the force balance acting on the hydraulic cylinder at any given moment is:

$$m_p \ddot{x}_{cy} = p_1 A_1 - p_2 A_2 - F_{ms} - F_n. \tag{7}$$

The frictional force (F_{ms}) is determined by the expression:

$$F_{ms} = f_v \cdot \dot{x}_{cy}. \tag{8}$$

The studies [11, 12, 21–23], have indicated the relationship between the pressure in the cylinder chambers and the displacement speed of the piston according to the following expressions:

$$\dot{p}_1 = \frac{E_o}{V_{01} + A_1 x_{cy}}\left(Q_1\left(p_1\right) - A_1 \dot{x}_{cy} - Q_3\left(p_1, p_2\right)\right); \tag{9}$$

$$\dot{p}_2 = \frac{E_o}{V_{02} + A_2 x_{cy}}\left(Q_2\left(p_2\right) + A_2 \dot{x}_{cy} + Q_3\left(p_1, p_2\right) - Q_4\left(p_2\right)\right). \tag{10}$$

Assuming no hydraulic oil leaks and the pressure in the piston rod chamber is constant, in that case $Q_3 = Q_4 = 0$. Because the displacement speed of the piston is very slow, the inertial effect of the piston is negligible. Therefore, the assumption is made to neglect the inertial force of the piston, meaning to disregard the $m_p \ddot{x}_{cyl}$. Q_1 is the constant oil flow rate into the cylinder. In this case, let's obtain the following result:

$$F_n = p_1 A_1 - p_2 A_2 - f_v \dot{x}_{cy}, \tag{11}$$

$$\dot{p}_1 = \frac{E_o}{V_{01} + A_1 x_{cy}}\left(Q_1 - A_1 \dot{x}_{cy}\right), \tag{12}$$

120

where

$$x_{cy} = S - S_0 + x_0 \Rightarrow \dot{x}_{cy} = \dot{S}. \tag{13}$$

S is the total length of the cylinder at any given time, S_0 is the initial total length of the cylinder, x_0 is the initial distance between the piston and the tail of the cylinder:

$$S = sqrt \left\{ \begin{array}{l} n_1{}^2 + n_2{}^2 + n_3{}^2 - 2n_1 n_2 \cos(\alpha_2 - \alpha_1) \\ +2n_1 n_3 \cos(\psi - \alpha_1) - 2n_2 n_3 \cos(\psi - \alpha_2) \end{array} \right\}, \tag{14}$$

$$\dot{S} = \frac{(n_2 n_3 \sin(\psi - \alpha_2) - n_1 n_3 \sin(\psi - \alpha_1))\dot{\psi}}{S}. \tag{15}$$

2. 2. 6. The system of differential equations

Apply the Lagrange's second kind equation to formulate the system of differential equations describing the oscillations of the system in the form:

$$\frac{d}{dt}\left(\frac{T}{\partial \dot{q}_i}\right) - \frac{\partial T}{\partial q_i} + \frac{\partial \Pi}{\partial q_i} + \frac{\partial \Phi}{\partial \dot{q}_i} = Q_i \ (i = 1 \div 4). \tag{16}$$

Substituting the expressions for kinetic energy, potential energy, and dissipative functions into equation (16), let's obtain the system of differential equations describing the oscillations of the system as follows:

$$m_1 \ddot{q} + (b_1 + b_2)\dot{q} - b_2 \dot{y} + b_2 f \dot{\varphi} + (k_1 + k_2)q - k_2 y + k_2 f \varphi + m_1 g = 0, \tag{17}$$

$$\begin{aligned} &(m_2 + m_s)\ddot{y} + m_s \left(n_1 \cos(\varphi + \alpha_1) + n_4 \cos(\varphi + \psi + \alpha_3)\right)\ddot{\varphi} + \\ &+ m_s n_4 \cos(\varphi + \psi + \alpha_3)\ddot{\psi} - m_s \left(n_1 \sin(\varphi + \alpha_1) + n_4 \sin(\varphi + \psi + \alpha_3)\right)\dot{\varphi}^2 - \\ &- b_2 \dot{q} + (b_2 + b_3)\dot{y} + (b_3 e - b_2 f)\dot{\varphi} - m_s n_4 \sin(\varphi + \psi + \alpha_3)(2\dot{\varphi} + \dot{\psi})\dot{\psi} - \\ &- k_2 q + (k_2 + k_3)y + (-k_2 f + k_3 e)\varphi + (m_2 + m_s)g = 0, \end{aligned} \tag{18}$$

$$\begin{aligned} &m_s \left(n_1 \cos(\varphi + \alpha_1) + n_4 \cos(\varphi + \psi + \alpha_3)\right)\ddot{y} + m_s \left(n_4{}^2 + n_1 n_4 \cos(\psi + \alpha_3 - \alpha_1)\right)\ddot{\psi} + \\ &+ \left(J_2 + m_s \left(n_1{}^2 + n_4{}^2 + 2n_1 n_4 \cos(\psi + \alpha_3 - \alpha_1)\right)\right)\ddot{\varphi} + (b_3 e - b_2 f)\dot{y} + b_2 f \dot{q} + \\ &+ \left(b_2 f^2 + b_3 e^2\right)\dot{\varphi} - m_s n_1 n_4 \sin(\psi + \alpha_3 - \alpha_1)(2\dot{\varphi} + \dot{\psi})\dot{\psi} + k_2 f q + (k_3 e - k_2 f)y + \\ &+ \left(k_2 f^2 + k_3 e^2\right)\varphi + m_s g \left(n_1 \cos(\varphi + \alpha_1) + n_4 \cos(\varphi + \psi + \alpha_3)\right) = 0, \end{aligned} \tag{19}$$

$$\begin{aligned} &m_s n_4 \cos(\varphi + \psi + \alpha_3)\ddot{y} + m_s \left(n_4{}^2 + n_1 n_4 \cos(\psi + \alpha_3 - \alpha_1)\right)\ddot{\varphi} + \left(J_s + m_s n_4{}^2\right)\ddot{\psi} + \\ &+ m_s n_1 n_4 \sin(\psi + \alpha_3 - \alpha_1)\dot{\varphi}^2 + m_s g n_4 \cos(\varphi + \psi + \alpha_3) = r\left(p_1 A_1 - p_2 A_2 - f_v \dot{x}_{cy}\right), \end{aligned} \tag{20}$$

$$\left(V_{01} + A_1 x_{cy}\right)\dot{p}_1 + E_o A_1 \dot{x}_{cy} = E_o Q_1. \tag{21}$$

The Matlab software application is used to solve a system of differential equations (17)–(21) with given initial conditions is:

$$\begin{bmatrix} q_0 & y_0 & \varphi_0 & \psi_0 & p_1 \end{bmatrix}^T = \begin{bmatrix} 0 & 0 & 0 & 2.512 & 12500000 \end{bmatrix}^T,$$

$$\begin{bmatrix} \dot{q}_0 & \dot{y}_0 & \dot{\varphi}_0 & \dot{\psi}_0 & \dot{p}_1 \end{bmatrix}^T = \begin{bmatrix} 0 & 0 & 0 & 0 & 0 \end{bmatrix}^T.$$

The Table of input parameters to solve the system of differential equations is in **Table 1**.

121

Table 1

Factors and value (all parameters are in SI-units)

Parameter	Value	Parameter	Value	Parameter	Value
e	2.24	k_1	800000	J_2	39252
f	5.62	k_2	295000	J_s	24558
n_1	5.36	k_3	10^7	E_o	169×10^7
n_2	3.83	α_1	0.052	V_{01}	0.00064
n_3	0.51	α_2	0.054	A_1	0.0128
n_4	2.8	α_3	0.3053	A_2	0.007
n_5	1.56	α_4	0.1483	p_2	3000000
b_1	500	m_1	910	f_v	240000
b_2	24000	m_2	8390	x_0	0.15
b_3	200	m_s	7800	Q_1	1.33×10^{-5}

3. Results and discussion

The simulation results are presented in the graphs in **Fig. 4**–**7**. Vertical displacement and velocity of the non-suspended front axle mass m_1 are represented in **Fig. 4**.
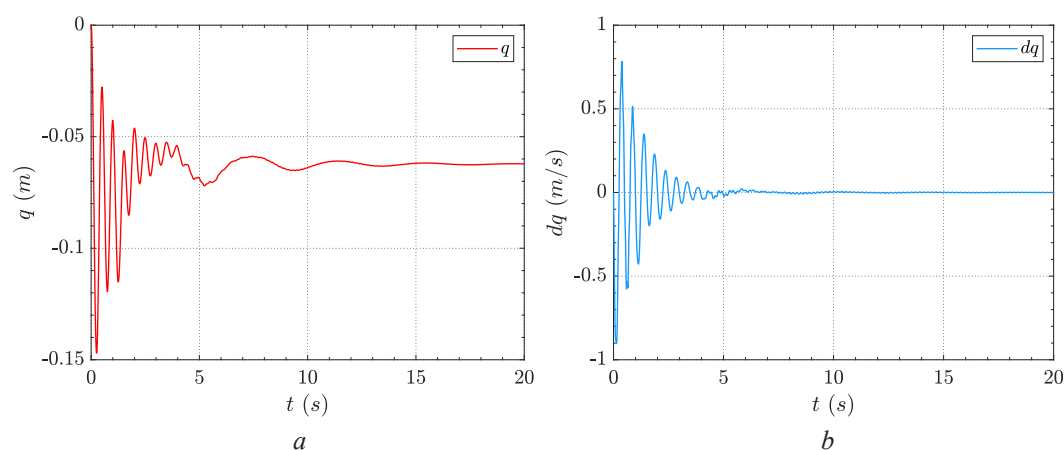
Fig. 4. Vibration of the center of mass of m_1: a – vertical displacement; b – vibration velocity

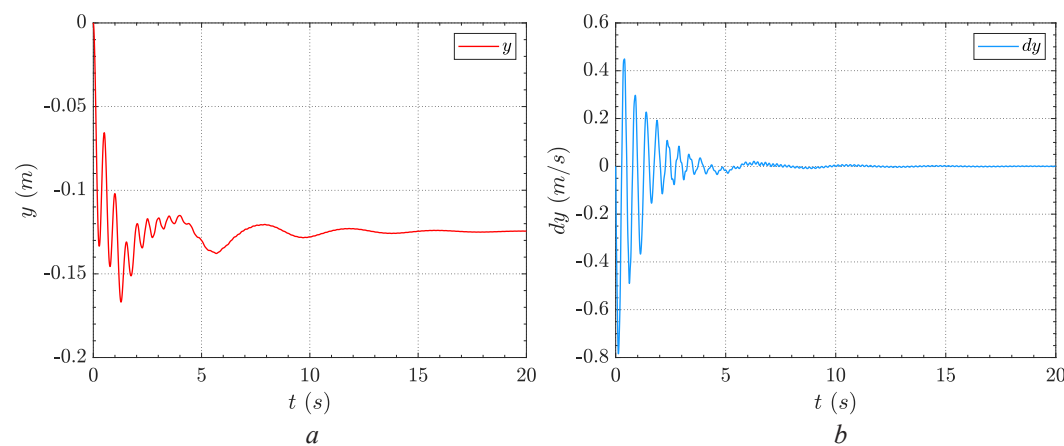Vertical displacement and velocity of the suspended mass on the vehicle chassis m_2 are represented in **Fig. 5**.

Fig. 5. Vibration of the center of mass of m_2: a – vertical displacement; b – vibration velocity

122

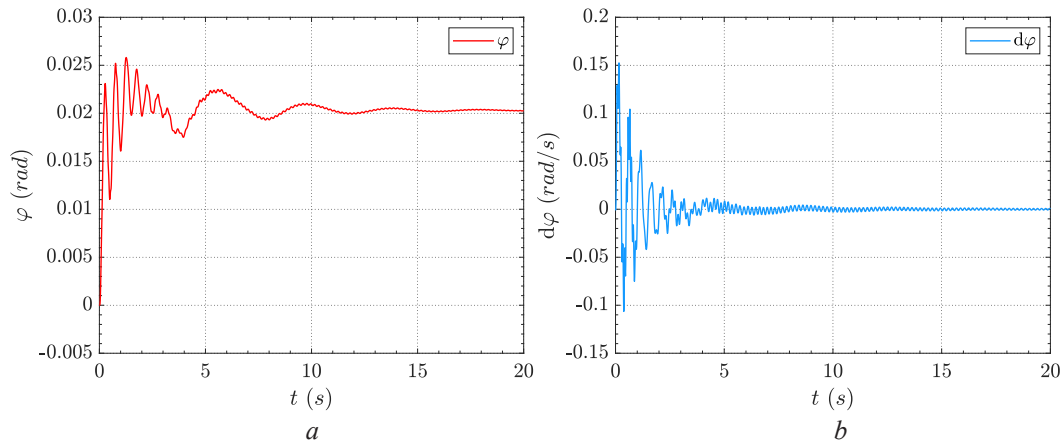Pitch angle and angular velocity of the chassis are represented in **Fig. 6**.

Fig. 6. Vibration of the chassis: *a* – pitch angle; *b* – angular velocity

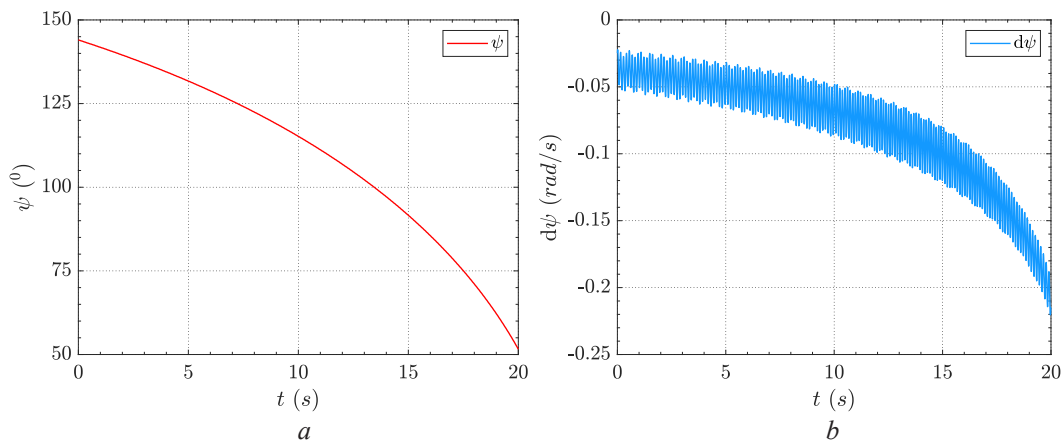Angular displacement and angular velocity of the bridge span block are represented in **Fig. 7**.

Fig. 7. Vibration of the mass of the bridge span block m_s:
a – angular displacement; *b* – angular velocity

The graph in **Fig. 4** illustrates the vertical displacement and oscillation velocity of the center of mass m_1 over time. It can be observed that the oscillation graph diminishes gradually, with a large amplitude during the initial 2 seconds and decreasing thereafter. The oscillation velocity approaches zero from the 5th second onward. During the stable working phase, the position of the center of mass m_1 is lower than the initial position by approximately 6.2 cm.

The graph in **Fig. 5** depicts the vertical displacement and oscillation velocity of the center of mass m_2 over time. The graph exhibits a gradually diminishing oscillation that stabilizes around the 7th second. At that point, the oscillation velocity approaches zero, and the position of the center of mass m_2 is lower than the initial position by approximately 13.5 cm. This diminishing oscillation is attributed to the damping system of the front suspension, which aids in damping the oscillation.

The graph in **Fig. 6** illustrates the angular displacement and angular velocity of the vehicle body around the axis passing through the center of mass m_2. The graph shows a gradually diminishing oscillation, with the maximum amplitude of angular displacement being approximately 1.5°. The correlation between the graphs in **Fig. 4, 5** with **Fig. 6** indicates that the angular oscillation of the vehicle body also follows a diminishing oscillation pattern consistent with the oscillation of m_1 and m_2.

The angular displacement and angular velocity of the bridge span block are depicted in the graph in **Fig. 7**. The initial value of the rotation angle ψ defining the position of the bridge span

123

block in the coordinate system considered above is 144°. The process of lifting the frame to raise the entire bridge span block is a process of gradually decreasing the rotation angle. At the end of the phase, the rotation angle ψ is 53°. The graph of the angular velocity $\dot{\psi}$ in **Fig. 7** shows that the angular velocity increases over time but at a slow rate. The variation of $\dot{\psi}$ over time is reflected in the graph of ψ not being a smooth curve. The theoretical problem mentioned above is solved with one of the input parameters being the constant flow of oil supplied to the cylinder chamber. However, in reality, this flow is not constant due to the control of the operator. If the oil flow to the cylinder is increased, the rotational speed of the bridge span block will also be faster.

The research focuses on the TMM-3M heavy mechanized bridge during its initial deployment phase. However, the results obtained are not sufficient to evaluate the overall process of complete bridge erection. Nonetheless, they hold theoretical significance in terms of calculations, serving to improve the overall performance of the TMM-3M bridge. The study reveals limitations in that it does not account for wind loads, the effects of soil elasticity, as well as the horizontal and vertical slopes of the ground on the lifting process. The TMM-3M bridge is military equipment that has been in production for a long time, thus its manufacturing technology may have limitations compared to current developments. Providing recommendations for operational efficiency, minimizing deployment time, reducing the number of personnel required for deployment, and enhancing the automation capabilities of the TMM-3M bridge are highly necessary and achievable through reasonable improvements in certain components and assemblies of this equipment such as the rear outriggers, hydraulic lifting system, and cable drive mechanism. To achieve these aims, the next areas of focus should involve studying the dynamics of the TMM-3M bridge during the opening span, lowering span, and lowering intermediate supports, taking into account the influence of wind loads and soil conditions to assess the overall deployment process of the equipment and find the most reasonable improvement solutions.

4. Conclusions

The article has presented a dynamic model and established a system of differential equations describing the oscillations of the TMM-3M heavy mechanized bridge during the frame lifting stage. The results indicate that the approximate completion time for the frame lifting process is around 20 seconds, with a damping time of oscillations of about 5 seconds from the initial moment. The article has analyzed the oscillations of the system during the lifting process, which align reasonably well with real-world working conditions. The content of the article has effectively addressed the integration of the mechanical-hydraulic model, demonstrating the pressure changes within the hydraulic cylinders in response to external loads. The achieved results of the article mark the beginning of a comprehensive study of the working process of the TMM-3M heavy mechanized bridge, potentially serving as theoretical groundwork for design calculations, improvements to the rear outriggers of the equipment, and control problems related to driving the hydraulic cylinders to increase the lifting speed of the bridge mass while maintaining necessary stability.

Conflict of interest

The authors declare that they have no conflict of interest in relation to this research, whether financial, personal, authorship or otherwise, that could affect the research and its results presented in this paper.

Financing

The study was performed without financial support.

Data availability

Manuscript has no associated data.

Use of artificial intelligence

The authors confirm that they did not use artificial intelligence technologies when creating the current work.

References

[1] Russell, B. R., Thrall, A. P. (2013). Portable and Rapidly Deployable Bridges: Historical Perspective and Recent Technology Developments. Journal of Bridge Engineering, 18 (10), 1074–1085. https://doi.org/10.1061/(asce)be.1943-5592.0000454

[2] Kalangi, Ms. C., Sidagam, Y. (2016). Design and Analysis of Armored Vehicle Launched Bridge (AVLB) for Static Loads. IJSRD – International Journal for Scientific Research & Development, 4 (10), 9–18. Available at: https://www.ijsrd.com/articles/IJSRDV4I100023.pdf

[3] Kim, Y. J., Tanovic, R., Wight, R. G. (2010). Load Configuration and Lateral Distribution of NATO Wheeled Military Trucks for Steel I-Girder Bridges. Journal of Bridge Engineering, 15 (6), 740–748. https://doi.org/10.1061/(asce)be.1943-5592.0000113

[4] Nor, N. M., (2011). Static analysis and design of sandwiched composite long-span portable beam. African Journal Of Business Management, 6 (27). https://doi.org/10.5897/ijps11.129

[5] Srividya, D. V., Raju, B., Kondayya, D. (2014). Design optimization of armored vehicle launched bridge for structural loads. International Journal of Mechanical Engineering, 2 (9).

[6] Szelka, J., Wysoczański, A. (2022). Modern structures of military logistic bridges. Open Engineering, 12 (1), 1106–1112. https://doi.org/10.1515/eng-2022-0391

[7] Han, J., Zhu, P., Tao, L., Chen, G., Zhang, S., Yang, X. (2019). An optimum design method for a new deployable mechanism in scissors bridge. Proceedings of the Institution of Mechanical Engineers, Part C: Journal of Mechanical Engineering Science, 233 (19-20), 6953–6966. https://doi.org/10.1177/0954406219869046

[8] Abdi, F., Qian, Z., Mosallam, A., Iyer, R., Wang, J.-J., Logan, T. (2006). Composite army bridges under fatigue cyclic loading. Structure and Infrastructure Engineering, 2 (1), 63–73. https://doi.org/10.1080/15732470500254691

[9] TMM-3. Available at: https://ru.wikipedia.org/wiki/TMM-3

[10] Baryshnikov, Y. N. (2018). Computing experiment for unloading dumper truck at a sloping pad. IOP Conference Series: Materials Science and Engineering, 468, 012022. https://doi.org/10.1088/1757-899x/468/1/012022

[11] Kang, Y. T., Yang, J., Zhang, W. M. (2012). Multi-Objective Optimization Design for Body Hoist Mechanism of Mining Dump Truck. Advanced Materials Research, 490-495, 396–401. https://doi.org/10.4028/www.scientific.net/amr.490-495.396

[12] Yan, T. P. (2012). The Air Controlled Hydraulic System Design of 3201z-Type Dump Truck Lifting Mechanisms. Advanced Materials Research, 433-440, 3852–3857. https://doi.org/10.4028/www.scientific.net/amr.433-440.3852

[13] Jiang, R. C., Liu, D. W., Wang, Z. C., Fan, W. (2012). Dynamic Characteristics Simulation for Lifting Mechanism of Dump Truck Based on Virtual Prototype. Applied Mechanics and Materials, 195-196, 754–757. https://doi.org/10.4028/www.scientific.net/amm.195-196.754

[14] Guan, Q., Gong, A., Hu, M., Liao, Z., Chen, X. (2020). Anti-Rollover Warning Control of Dump Truck Lifting Operation Based on Active Suspension. Journal of Control, Automation and Electrical Systems, 32 (1), 109–119. https://doi.org/10.1007/s40313-020-00664-y

[15] Grigorov, B., Mitrev, R. (2017). Dynamic behavior of a hydraulic crane operating a freely suspended payload. Journal of Zhejiang University-SCIENCE A, 18 (4), 268–281. https://doi.org/10.1631/jzus.a1600292

[16] Jensen, K. J., Ebbesen, M. K., Hansen, M. R. (2021). Anti-swing control of a hydraulic loader crane with a hanging load. Mechatronics, 77, 102599. https://doi.org/10.1016/j.mechatronics.2021.102599

[17] Ikonen, T. (2006). Bucket and Vehicle Oscillation Damping for a Wheel Loader. Lund University. Available at: https://lup.lub.lu.se/student-papers/search/publication/8847851

[18] Tuan, L. A. (2019). Fractional-order fast terminal back-stepping sliding mode control of crawler cranes. Mechanism and Machine Theory, 137, 297–314. https://doi.org/10.1016/j.mechmachtheory.2019.03.027

[19] Duong, L. V., Tuan, L. A. (2022). Modeling and observer-based robust controllers for telescopic truck cranes. Mechanism and Machine Theory, 173, 104869. https://doi.org/10.1016/j.mechmachtheory.2022.104869

[20] Tuan, L. A., Lee, S.-G. (2018). Modeling and advanced sliding mode controls of crawler cranes considering wire rope elasticity and complicated operations. Mechanical Systems and Signal Processing, 103, 250–263. https://doi.org/10.1016/j.ymssp.2017.09.045

[21] Jaiswal, S., Sopanen, J., Mikkola, A. (2021). Efficiency comparison of various friction models of a hydraulic cylinder in the framework of multibody system dynamics. Nonlinear Dynamics, 104 (4), 3497–3515. https://doi.org/10.1007/s11071-021-06526-9

[22] Linjama, M., Virvalo, T. (1999). Low-order dynamic model for flexible hydraulic cranes. Proceedings of the Institution of Mechanical Engineers, Part I: Journal of Systems and Control Engineering, 213 (1), 11–22. https://doi.org/10.1243/0959651991540340

[23] Ruderman, M., Kaltenbacher, S., Horn, M. (2021). Pressure-flow dynamics with semi-stable limit cycles in hydraulic cylinder circuits. 2021 IEEE International Conference on Mechatronics (ICM). https://doi.org/10.1109/icm46511.2021.9385620

Engineering